Double-layer graphene and topological insulator thin-film plasmons

Rosario E. V. Profumo,[1] Reza Asgari,[2,*] Marco Polini,[3,†] and A. H. MacDonald[4]
[1]*Dipartimento di Fisica dell'Università di Pisa and NEST, Istituto Nanoscienze-CNR, I-56127 Pisa, Italy*
[2]*School of Physics, Institute for Research in Fundamental Sciences (IPM), Tehran 19395-5531, Iran*
[3]*NEST, Istituto Nanoscienze-CNR and Scuola Normale Superiore, I-56126 Pisa, Italy*
[4]*Department of Physics, University of Texas at Austin, Austin, Texas 78712, USA*
(Received 20 December 2011; published 29 February 2012)

We present numerical and analytical results for the optical and acoustic plasmon collective modes of coupled massless-Dirac two-dimensional electron systems. Our results apply to topological insulator (TI) thin films and to two graphene sheets separated by a thin dielectric barrier layer. We find that, because of strong bulk dielectric screening, TI acoustic modes are locked to the top of the particle-hole continuum and, therefore, probably unobservable.

DOI: 10.1103/PhysRevB.85.085443 PACS number(s): 73.21.Ac, 73.20.Mf

I. INTRODUCTION

The physics of closely spaced but unhybridized two-dimensional electron systems (2DESs) has been a subject of theoretical and experimental interest since it was first appreciated[1,2] that electron-electron interactions allow energy and momentum to be transferred between layers, while maintaining separate particle-number conservation. Remote Coulomb coupling has commanded a great deal of attention during the past 30 years or so because it provides a potential alternative to the inductive and capacitive coupling of conventional electronics. Until recently, remote Coulomb coupling research focused on quasi-2D electron systems confined to nearby quantum wells in molecular-beam-epitaxy grown semiconductor heterostructures. The study of Coulomb-coupled 2D systems has now been revitalized by advances that have made it possible to prepare robust and ambipolar 2DESs, based on graphene[3] layers or on the surface states of topological insulators[4] that are described by an ultrarelativistic wave equation instead of the nonrelativistic Schrödinger equation.

Single- and few-layer graphene systems can be produced by mechanical exfoliation of thin graphite or by thermal decomposition of silicon carbide.[5] Isolated graphene layers host massless-Dirac two-dimensional electron systems (MD2DESs) with a fourfold (spin × valley) flavor degeneracy, whereas topologically protected MD2DESs that have no additional spin or valley flavor labels appear automatically[4,6] at the top and bottom surfaces of a three-dimensional (3D) topological insulator (TI) thin film. The protected surface states of 3D TIs are associated with spin-orbit interaction driven bulk band inversions. 3D TIs in a slab geometry offer two surface states that can be far enough apart to make single-electron tunneling negligible but close enough for Coulomb interactions between surfaces to be important. Unhybridized MD2DES pairs can be realized in graphene by separating two layers by a dielectric[7] (such as Al_2O_3) or by a few layers of a one-atom-thick insulator such as BN.[8,9] In both cases interlayer hybridization is negligible and the nearby graphene layers are, from the point of view of single-particle physics, isolated. Isolated graphene layers can be also found on the surface of bulk graphite[10,11] and in "folded graphene"[12] (a natural byproduct of micromechanical exfoliation) or prepared by chemical vapor deposition.[11] We use the term *double-layer graphene* (DLG) to refer to a system with two graphene layers that are coupled only by Coulomb interactions, avoiding the term *bilayer graphene*, which typically refers to two adjacent graphene layers in the crystalline Bernal-stacking configuration.[13]

DLG and TI thin films are both described at low energies by a Hamiltonian with two MD2DES[3] coupled only by Coulomb interactions. The importance of electron-electron interactions in MD2DESs has been becoming more obvious as sample quality has improved,[14] motivating investigations of charge and spin or pseudospin dynamics in DLG and thin-film TIs in the regime in which long-range Coulomb forces give rise to robust plasmon collective modes.[15,16] Because of their electrically tunable collective behaviors, DLG and thin-film TIs may have a large impact on *plasmonics*, a very active subfield of optoelectronics[17–19] whose aim is to exploit plasmon properties in order to compress infrared electromagnetic waves to the nanometer scale of modern electronic devices.

In this paper we use the random-phase approximation (RPA)[15,16] to evaluate the optical and acoustic plasmon mode dispersions in DLG and in thin-film TIs. In particular, we obtain an *exact* analytical formula for the RPA acoustic plasmon group velocity valid for arbitrary substrate and barrier dielectrics that points to a key difference between these two MD2DES's, namely that the velocity in TI thin films is strongly suppressed. The RPA collective modes of DLG have been calculated earlier by Hwang and Das Sarma;[20] Below we will comment at length on the relation between our results and theirs. Plasmon collective modes formed from TI surface states have also been considered previously by Raghu *et al.*[21] in the regime in which coupling between top and bottom surfaces can be neglected. Based on our analysis, we are able to clarify how dielectric screening influences plasma frequencies in this limit. Finally, we wish to mention that the role of optical and acoustic plasmon modes in relation to DLG exciton condensates has been studied in Ref. 22.

Plasmons can be observed by a variety of experimental tools, including inelastic light scattering,[23] which has been widely used to probe plasmons in semiconductor heterostructures,[24] but also by surface-physics techniques like high-resolution electron-energy-loss spectroscopy[25] and, more indirectly, angle-resolved photoemission spectroscopy.[14]

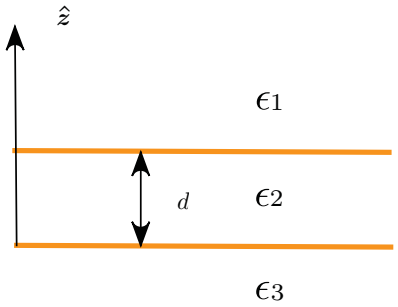

FIG. 1. (Color online) A side view of the double-layer system described by Eq. (1), which explicitly indicates the dielectric model used in these calculations. The two layers hosting massless Dirac fermions are located at $z = 0$ and $z = d$.

Double-layer field-effect transistors with a grating gate[26] can also be used to detect plasmons. Coupling between far-infrared light and Dirac plasmons in single-layer graphene has recently been achieved by employing an array of graphene nanoribbons[27] and by performing near-field scanning optical microscopy through the tip of an AFM.[28]

This paper is organized as follows. In Sec. II we present the model we have used to describe a pair of Coulomb-coupled MD2DESs and introduce the linear-response functions that describe collective electron dynamics. In Sec. III we present and discuss our main analytical and numerical results for the dispersion of optical and acoustic plasmons in these systems. Finally, in Sec. IV we present a summary of our main conclusions.

II. MODEL HAMILTONIAN AND RANDOM-PHASE APPROXIMATION

We consider two unhybridized MD2DESs separated by a finite distance d and embedded in the dielectric environment depicted in Fig. 1. The two systems are assumed to be coupled solely by Coulomb interactions. The Hamiltonian describing this system reads[29] ($\hbar = 1$)

$$\hat{\mathcal{H}} = v \sum_{\boldsymbol{k},\ell,\alpha,\beta} \hat{\psi}^{\dagger}_{\boldsymbol{k},\ell,\alpha} (\boldsymbol{\sigma}_{\alpha\beta} \cdot \boldsymbol{k}) \hat{\psi}_{\boldsymbol{k},\ell,\beta} + \frac{1}{2S} \sum_{\boldsymbol{q},\ell,\ell'} V_{\ell\ell'}(q) \hat{\rho}_{\boldsymbol{q},\ell} \hat{\rho}_{-\boldsymbol{q},\ell'}, \quad (1)$$

where v is the bare Dirac velocity, taken to be the same in the $\ell = 1,2$ tunnel-decoupled layers, S is the area of each layer, $V_{\ell\ell'}(q)$ is the matrix of bare Coulomb potentials, and

$$\hat{\rho}_{\boldsymbol{q},\ell} = \sum_{\boldsymbol{k},\alpha} \hat{\psi}^{\dagger}_{\boldsymbol{k}-\boldsymbol{q},\ell,\alpha} \hat{\psi}_{\boldsymbol{k},\ell,\alpha} \quad (2)$$

is the density-operator for the ℓ-th layer. The Greek letters are honeycomb-sublattice-pseudospin labels and $\boldsymbol{\sigma} = (\sigma^x, \sigma^y)$ is a vector of Pauli matrices. A sum over flavor labels is implicit in Eq. (2) in the case of DLG. The relative strength of Coulomb interactions is measured by the dimensionless coupling constant[3] (restoring $\hbar$ for a moment) $\alpha_{\rm ee} \equiv e^2/(\hbar v)$ which has a value $\approx$2.2 in DLG and $\approx$4.4 in Bi_2Te_3 TIs if we use the respective Dirac velocities $v_G \approx 10^6$ m/s and $v_{\rm TI} \approx 5 \times 10^5$ m/s.

Several important many-body properties of the Hamiltonian $\hat{\mathcal{H}}$ are completely determined by the 2×2 symmetric matrix $\boldsymbol{\chi}(q,\omega)$ whose elements are the density-density linear-response functions

$$\chi_{\ell\ell'}(q,\omega) = \frac{1}{S} \langle\langle \hat{\rho}_{\boldsymbol{q},\ell}; \hat{\rho}_{-\boldsymbol{q},\ell} \rangle\rangle_{\omega}, \quad (3)$$

with $\langle\langle \hat{A}, \hat{B} \rangle\rangle_{\omega}$ the usual Kubo product.[16] Within the RPA these functions satisfy the following matrix equation:

$$\boldsymbol{\chi}^{-1}(q,\omega) = \boldsymbol{\chi}_0^{-1}(q,\omega) - \boldsymbol{V}(q), \quad (4)$$

where $\boldsymbol{\chi}_0(q,\omega)$ is a 2×2 diagonal matrix whose elements $\chi^{(0)}_{\ell}(q,\omega)$ are the well-known[30–32] noninteracting (Lindhard) response functions of each layer at arbitrary doping n_{ℓ}. The off-diagonal (diagonal) elements of the matrix $\boldsymbol{V} = \{V_{\ell\ell'}\}_{\ell,\ell'=1,2}$ represent interlayer (intralayer) Coulomb interactions.

The bare intra- and interlayer Coulomb interactions are influenced by the layered dielectric environment (see Fig. 1). A simple electrostatic calculation[29] implies that the Coulomb interaction in the $\ell = 1$ (top) layer is given by

$$V_{11}(q) = \frac{4\pi e^2}{q D(q)} [(\epsilon_2 + \epsilon_3) e^{qd} + (\epsilon_2 - \epsilon_3) e^{-qd}], \quad (5)$$

where

$$D(q) = [(\epsilon_1 + \epsilon_2)(\epsilon_2 + \epsilon_3) e^{qd} + (\epsilon_1 - \epsilon_2)(\epsilon_2 - \epsilon_3) e^{-qd}]. \quad (6)$$

The Coulomb interaction in the bottom layer, $V_{22}(q)$, can be simply obtained from $V_{11}(q)$ by interchanging $\epsilon_3 \leftrightarrow \epsilon_1$. Finally, the interlayer Coulomb interaction is given by

$$V_{12}(q) = V_{21}(q) = \frac{8\pi e^2}{q D(q)} \epsilon_2. \quad (7)$$

Note that in the "uniform" $\epsilon_1 = \epsilon_2 = \epsilon_3 \equiv \epsilon$ limit we recover the familiar expressions $V_{11}(q) = V_{22}(q) \to 2\pi e^2/(\epsilon q)$ and $V_{12}(q) = V_{21}(q) \to V_{11}(q) \exp(-qd)$. Previous work on TI thin-film and DLG collective modes has assumed this limit, which rarely applies experimentally.

III. COLLECTIVE MODES

The collective modes of the system described by the model Hamiltonian (1) can be determined by locating the poles of $\boldsymbol{\chi}(q,\omega)$ in Eq. (4). A straightforward inversion of Eq. (4) yields the following condition:[33,34]

$$\varepsilon(q,\omega) = \left[1 - V_{11}(q)\chi^{(0)}_1(q,\omega)\right]\left[1 - V_{22}(q)\chi^{(0)}_2(q,\omega)\right] - V^2_{12}(q)\chi^{(0)}_1(q,\omega)\chi^{(0)}_2(q,\omega) = 0. \quad (8)$$

The collective modes occur above the intraband particle-hole continuum where $\chi^{(0)}$ is real, positive, and a decreasing function of frequency. Equation (8) admits two solutions, a higher-frequency solution[30,31,35] at $\omega_{\rm op}(q)$ that corresponds to in-phase oscillations of the densities in the two layers and a lower-frequency solution at $\omega_{\rm ac}(q)$ that corresponds to out-of-phase oscillations.

The plasmon collective modes of MD2DESs are of special interest because of the ease with which they may be altered by changing the carrier densities in either layer using gates. We note, in particular, that the carrier densities in different

layers can easily differ radically. For this reason, we present our results in terms of the total 2D carrier density $n = n_1 + n_2$ and the density polarization $\zeta = (n_2 - n_1)/n \in [-1,1]$: $\zeta = 1$ when the carrier density is nonzero only in the bottom layer ($n_1 = 0$), while $\zeta = 0$ when the two layers have identical carrier densities ($n_1 = n_2$).

A. Analytical results

In this section we report on exact analytical expressions for the RPA optical and acoustic plasmon dispersions $\omega_{\mathrm{op,ac}}(q)$ that are valid in the long-wavelength $q \to 0$ limit where $\omega_{\mathrm{op}}(q \to 0) \propto \sqrt{q}$ and $\omega_{\mathrm{ac}}(q \to 0) \propto q$.

We start by deriving an exact expression for the RPA long-wavelength acoustic-plasmon group velocity,

$$c_{\mathrm{s}} = \lim_{q\to 0} \frac{\omega_{\mathrm{ac}}(q)}{q}. \tag{9}$$

Following Santoro and Giuliani,[34] we, first, introduce the power expansion

$$\omega_{\mathrm{ac}}(q) = c_{\mathrm{s}} q + c_2 q^2 + c_3 q^3 + \cdots \tag{10}$$

for the acoustic-plasmon dispersion relation and then define a function

$$F(q) = \varepsilon(q, c_{\mathrm{s}} q + c_2 q^2 + c_3 q^3 + \cdots). \tag{11}$$

In the limit $q \to 0$ the function $F(q)$ has the following Laurent-Taylor expansion:

$$F(q) = f_{-1} q^{-1} + f_0 + f_1 q + f_2 q^2 + \cdots, \tag{12}$$

where the coefficients f_i can be extracted from the analytical expression[30–32] for the MD2DES Lindhard function $\chi_\ell^{(0)}(q,\omega)$. For Eq. (8) to be valid we have to require that the coefficients f_i vanish identically. The coefficient f_{-1} depends only on c_s and by equating its expression to zero we arrive after some tedious but straightforward algebra at the following equation for $x = c_s/v$, the ratio between the plasmon group velocity c_s and the Dirac velocity v:

$$\begin{aligned} &2 g_s g_v \alpha_{\mathrm{ee}} \bar{d} (\zeta^2 - 1)[1 + 2x(\sqrt{x^2 - 1} - x)] \\ &\quad - \sqrt{2}\epsilon_2 [1 + x(\sqrt{x^2 - 1} - x)] f(\zeta) = 0, \end{aligned} \tag{13}$$

where g_s (g_v) are real-spin (valley) degeneracy factors. In the case of DLG, $g_s = g_v = 2$, while in the case of thin-film TIs $g_s = g_v = 1$. In Eq. (13) $\bar{d} = d k_F$ is a dimensionless interlayer distance calculated with $k_F \equiv \sqrt{4\pi n/(g_s g_v)}$ and $n = n_1 + n_2$ and

$$f(\zeta) = (1 + \zeta)\sqrt{1 - \zeta} + (1 - \zeta)\sqrt{1 + \zeta}. \tag{14}$$

Equation (13) can be conveniently solved for x by making the change of variables $x \mapsto \Gamma = \sqrt{x^2 - 1} - x$. After some straigthforward algebra we find that

$$\frac{c_s}{v} = \frac{1 + \Lambda(\alpha_{\mathrm{ee}} \bar{d}/\epsilon_2, \zeta)}{[1 + 2\Lambda(\alpha_{\mathrm{ee}} \bar{d}/\epsilon_2, \zeta)]^{1/2}} \tag{15}$$

with

$$\Lambda(\alpha_{\mathrm{ee}} \bar{d}/\epsilon_2, \zeta) = \frac{g_s g_v \sqrt{2}(1 - \zeta^2)}{f(\zeta)} \frac{\alpha_{\mathrm{ee}} \bar{d}}{\epsilon_2}. \tag{16}$$

Equations (15) and (16) are the principle results of this paper. We see from this analytic expression that c_s is independent of ϵ_1 and ϵ_3 and depends only on the barrier material dielectric constant, which in the case of TI thin films is simply the TI bulk dielectric constant. This behavior is a consequence of the out-of-phase character of this collective mode in which the double-layer total charge is locally constant but shifts dynamically between layers. Because TIs tend to have narrow gaps they tend to have large dielectric constants ($\epsilon_2 \sim 100$ in the case[36] of Bi_2Te_3). Thin-film collective modes will, therefore, tend to have c_s/v values that are quite close to 1 unless $\bar{d}$ is very large. (For large $\bar{d}$ the long-wavelength limit formula, which applies when both qd and q/k_F are small, will have a limited range of applicability.)

It follows from Eq. (15) that the ratio c_s/v is larger than unity for any value of the parameters α_{ee}, $\bar{d}$, ζ, and ϵ_2 so the acoustic plasmon always lies outside of the MD2DES particle-hole continuum. This implies than the acoustic plasmon is, strictly speaking, never Landau damped at small q. (A similar conclusion was reached previously[34] for the case of conventional 2D electron gases but was limited to the case of identical density and, hence, identical Fermi velocity.)

For moderate values of $\bar{d}$, however, Eq. (15) predicts a TI thin-film sound velocity so close to the top of the particle-hole continuum that it will likely be unobservable because of damping effects not captured by the RPA and because of disorder, which is always present to some degree. For the case of DLG, on the other hand, we expect that acoustic plasmon collective modes will be well defined. This is particularly true in the case of DLG with a small number of layers of BN as barrier material. When the BN barrier layer is very thin, the use of macroscopic dielectric parameters to characterize its screening properties is approximate; in that case, measurement of the acoustic plasmon group velocity combined with Eqs. (15) and (16) would allow the effective value of ϵ_2 to be determined experimentally.

We note that an analytic result for c_{s} was reported previously in Ref. 20 [see their Eq. (5b)] for the special case of DLG embedded in a uniform dielectric, i.e., for $\epsilon_1 = \epsilon_2 = \epsilon_3$. In our notation, their result reads

$$\frac{c_{\mathrm{s}}}{v}\Big|_{\mathrm{HDS}} = \left[\frac{2\sqrt{2}\sqrt{1 - \zeta^2}}{\sqrt{1 - \zeta} + \sqrt{1 + \zeta}} \frac{\alpha_{\mathrm{ee}} \bar{d}}{\epsilon_2}\right]^{1/2}. \tag{17}$$

This equation evidently differs from Eq. (15) above. We believe that Eq. (15) is the correct RPA result for the acoustic-plasmon group velocity and that Eq. (17) is incorrect. The difference is due to the singular behavior of the Lindhard function $\chi_\ell^{(0)}(q,\omega)$ as a function of wave vector q and frequency ω in the region in which both these quantities are small. (See Sec. 4.4.3 of Ref. 16.) In particular, the limit of $\chi_\ell^{(0)}(q,\omega)$ for $q \to 0$ and $\omega \to 0$ depends on the ratio $\nu = \omega/(vq)$, i.e., on the direction along which the origin of the (q,ω) plane is approached: different limits are obtained for different values of ν. In an acoustic plasmon, the ratio ν approaches a constant as $q \to 0$ and, thus, the limit of $\chi_\ell^{(0)}(q,\omega)$ that matters is the one in which $q \to 0$ while the ratio ω/q is kept constant. This is the limit we have taken[34] in the derivation of Eq. (15) [see Eq. (11)]. Equation (17) is obtained by incorrectly letting $q \to 0$ while ω is kept constant [see Eq. (4) in Ref. 20]: In this limit ν *diverges*

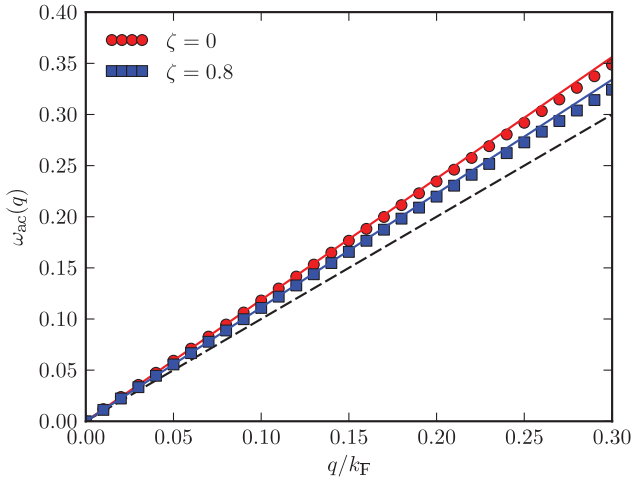

FIG. 2. (Color online) Long-wavelength acoustic plasmon dispersion of Coulomb-coupled massless-Dirac two-dimensional electron systems. The circles and squares are acoustic plasmon frequencies $\omega_{ac}(q)$ (in units of $\varepsilon_F = vk_F$) as functions of q/k_F calculated numerically from the solution of Eq. (8). Here k_F is the Fermi wave vector evaluated at the total density $n = n_1 + n_2$, i.e., $k_F = \sqrt{4\pi(n_1+n_2)/(g_s g_v)}$. The parameters we have used to calculate the curve labeled by "$\zeta = 0$" are $g_s = g_v = 2, n_1 = n_2 = 5 \times 10^{12}$ cm^{-2}, $\alpha_{ee} = 2.2$, $d = 3.35$ Å, $\epsilon_1 = \epsilon_2 = 1$, and $\epsilon_3 = 3.9$. These parameter values correspond to the case of two graphene layers on SiO_2 that are decoupled by rotation. The data labeled by "$\zeta = 0.8$" have been calculated by setting $n_1 = 1 \times 10^{12}$ cm^{-2} and $n_2 = 9 \times 10^{12}$ cm^{-2} with the same values for the other parameters. The solid lines plot $\omega = c_s q$ for the $\zeta = 0$ and $\zeta = 0.8$ cases with the plasmon group velocity c_s calculated from the analytical result, Eq. (15). These numerical results confirm the validity of our analytic result for c_s and the importance of accounting for the delicate dependence of the long-wavelength Lindhard function on $v = \omega/(vq)$. The dashed line plots the upper-bound of the intraband electron-hole continuum, $\omega = vq$.

instead of going to a constant value. A careful comparison between our analytical prediction in Eq. (15) and the result obtained by the brute-force numerical solution of Eq. (8) is shown in Fig. 2. We clearly see that Eq. (15) compares very well with the full numerical result.

The analytical analysis of the long-wavelength optical plasmon mode is simpler since this mode satisfies $\omega_{op}(q) \propto \sqrt{q}$ for $q \to 0$ and, therefore, occurs at $v = \omega/(vq) \to \infty$. We obtain an analytic result using the well-known high-frequency ($\omega \gg vq$ and $\omega \ll 2\varepsilon_{F,\ell}$) dynamical limit of $\chi_\ell^{(0)}(q,\omega)$:

$$\lim_{q\to 0} \chi_\ell^{(0)}(q,\omega) = g_s g_v \frac{\varepsilon_{F,\ell}}{4\pi} \frac{q^2}{\omega^2}, \tag{18}$$

with $\varepsilon_{F,\ell} = vk_{F,\ell} = v\sqrt{4\pi n_\ell/(g_s g_v)}$. Using Eq. (18) in Eq. (8) we immediately find

$$\omega_{op}^2(q \to 0) = \frac{g_s g_v \alpha_{ee}}{2\bar{\epsilon}} v^2 k_F \left(\sqrt{\frac{1+\zeta}{2}} + \sqrt{\frac{1-\zeta}{2}}\right) q, \tag{19}$$

with $\bar{\epsilon} = (\epsilon_1 + \epsilon_3)/2$. Note that Eq. (19) does not depend on the interlayer distance or on the dielectric constant ϵ_2, but only on the average $\bar{\epsilon}$ between top and bottom dielectric constants.

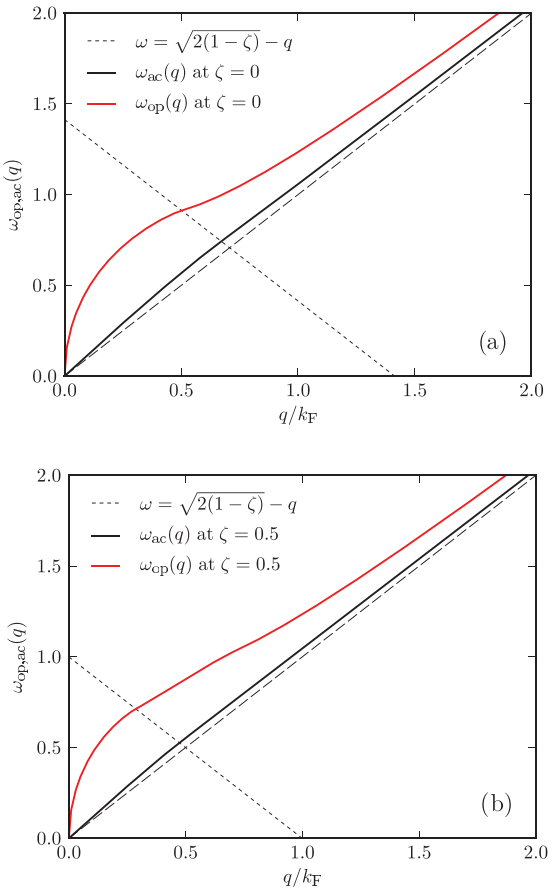

FIG. 3. (Color online) (a) Optical and acoustic plasmon dispersions (in units of the Fermi energy $\varepsilon_F = vk_F$) in a twisted double-layer graphene system on a SiO_2 substrate as functions of wave vector q [in units of $k_F = \sqrt{4\pi(n_1+n_2)/(g_s g_v)}$]. The values of the parameters that we have used to produce the data in this figure are $g_s = g_v = 2$, $n_1 = n_2 = 5 \times 10^{12}$ cm^{-2} (corresponding to $n = 10^{13}$ cm^{-2} and $\zeta = 0$), $\alpha_{ee} = 2.2$, $d = 3.35$ Å, $\epsilon_1 = \epsilon_2 = 1$, and $\epsilon_3 = 3.9$. The intersections between the plasmon dispersions and the short-dashed line give the critical wave vector q_c at which Landau damping starts. (b) Same as in panel (a) but for $\zeta = 0.5$ [in producing the data shown in panel (b) we have fixed the total density at the value used to produce the data in panel (a), *i.e.* $n = 10^{13}$ cm^{-2}].

Note also that, in the limit $n_1 \to 0$ ($\zeta = 1$), Eq. (19) reduces to the well-known plasmon frequency in a single-layer graphene sheet[30,31,35] with electron density n_2. This expression applies for $qd \ll 1$, in which case the entire double-layer MD2DES acts in the optical plasmon mode like a single conducting layer at the interface between dielectric media characterized by constants ϵ_1 and ϵ_3.

B. Numerical results

In this section we briefly report some representative numerical results for the optical and acoustic plasmon dispersion relations obtained by solving Eq. (8), discussing, first, DLG and then TI thin films.

In Fig. 3 we illustrate the typical properties of DLG plasmon modes for the case with the smallest MD2DES separation, two adjacent layers on a SiO_2 substrate ($\epsilon_1 = \epsilon_2 = 1$ and $\epsilon_3 = 3.9$) that are weakly hybridized, e.g., because of a twist

between their orientations.[37] Figure 3(a) is for a symmetric system with the same electron concentration on the two layers ($\zeta = 0$), while Fig. 3(b) refers to a system with a 50% density imbalance. The characteristic behaviors $\omega_{\rm op}(q) \propto \sqrt{q}$ of the optical plasmon and $\omega_{\rm ac}(q) \propto q$ of the acoustic plasmon are clearly visible. The collective modes are not Landau damped when they appear in the gap between intraband and interband particle-hole continua. When the two layers have different densities, their particle-hole continua differ and the gap is smaller for the lower density layer. For adjacent but twisted DLG systems $\bar{d}$ is small even when the carrier density is large ($\bar{d} \approx 0.2$ in Fig. 3). It follows that qd is small and the two MD2DESs are strongly coupled over the entire relevant frequency regime. In this small $\bar{d}$ example the acoustic plasmon frequency is close to the particle-hole continuum because the capacitive energy associated with charge sloshing between the layers is proportional to the small layer separation.

In Fig. 4 we illustrate the strength of plasmon decay by emission of single electron-hole pairs (Landau damping). Note that Landau damping occurs when the curves $\omega_{\rm op,ac}(q)$ in Fig. 3 hit the interband electron-hole continuum of the layer with lower density (layer "1" in our convention). The larger ζ, the sooner this happens. In particular, in the limit in which layer "1" is neutral ($\zeta = 1$), Landau damping is present from vanishingly small wave vectors: damping of the optical plasmon excitation associated with electrons in the high-density layer starts at arbitrarily small wave vectors since decay can easily occur *via* the emission of interband electron-hole pairs in the neutral layer. The many-body properties of two or more decoupled graphene layers thus can be strongly affected by interlayer Coulomb interactions, even by apparently innocuous geometric features such as the presence of a nearly neutral layer.

In Fig. 5 we compare optical and acoustic plasmon dispersions for DLG and TI thin-film systems. For the TI thin-film case we have chosen the following parameters: (i) $\epsilon_1 = 1$, $\epsilon_2 = 100$ (this roughly corresponds to the dielectric constant of Bi_2Te_3), and $\epsilon_3 = 4.0$; (ii) a total electron density on the top and bottom surface states of $n = 10^{13}$ cm^{-2}; and (iii) a thickness of the TI slab of $d = 6$ nm, corresponding to a six quintile layer MBE-grown Bi_2Te_3 film ($\bar{d} \approx 6.7$). The DLG example has the same total density and layer separation ($\bar{d} \approx 3.4$; the difference in $\bar{d}$ in the two cases stems from the g_s/g_v spin/valley degeneracy factors) and dielectric constants $\epsilon_1 = 1$ and $\epsilon_2 = \epsilon_3 = 4.0$, corresponding to two graphene layers separated by approximately 15 BN layers and lying on a BN substrate. In both cases we see that a crossover occurs at intermediate values of q between strong (small q) and weak (large q) coupling of the two collective modes. In the TI case the higher frequency optical plasmon mode deviates much more strongly from simple $\sqrt{q}$ behavior at this crossover because strong dielectric screening by the TI bulk suppresses the single-surface plasmon mode. [Note however that the effective dielectric constant for this limit is $(\epsilon_2 + \epsilon_{1,3})/2$ rather than ϵ_2 as used in Ref. 21.] The acoustic plasmon mode of the TI thin film case is, on the other hand, strongly suppressed in the strong-coupling limit, as discusses earlier, and has a velocity much closer to the bare Dirac velocity than in the corresponding DLG case.

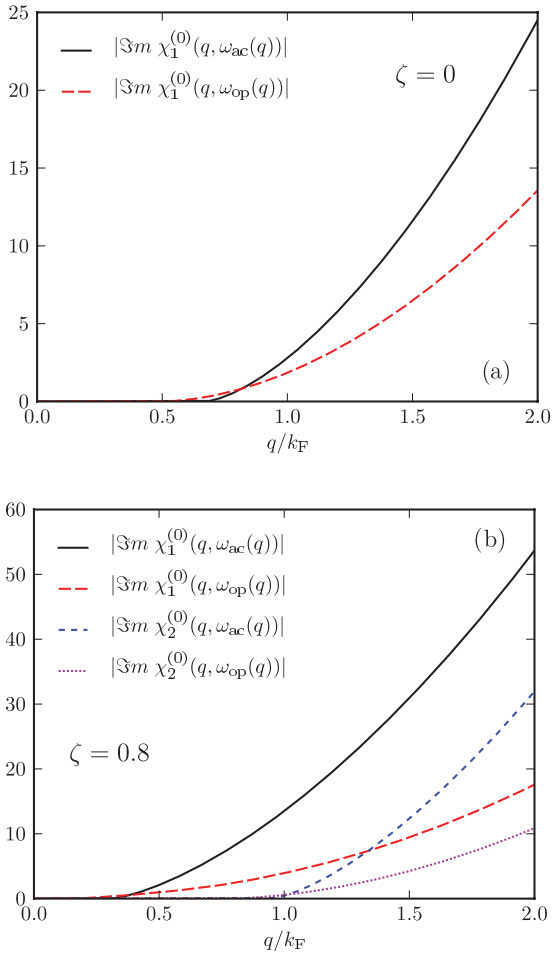

FIG. 4. (Color online) Landau damping of collective modes in double-layer graphene. (a) The absolute value of the imaginary part of the Lindhard function of the top layer, $|\Im m \chi_1^{(0)}(q,\omega)|$, evaluated at the frequency $\omega = \omega_{\rm op}(q)$ [$\omega = \omega_{\rm ac}(q)$] of the optical [acoustic] plasmon. The data in this plot refer exactly to the parameters used in Fig. 3(a). Note that, within RPA, $\Im m \chi_1^{(0)}(q,\omega_{\rm op,ac}(q))$ is identically zero for wave vectors q up to a critical value $q^{\star}_{\rm op,ac}$ at which $\omega_{\rm op,ac}(q)$ hits the interband electron-hole continuum associated with the low-density layer. Since data in this panel correspond to $\zeta = 0$, top-layer and bottom-layer Lindhard functions are identical. (b) Same as in panel (a) but for $\zeta = 0.8$ ($n_1 = 1 \times 10^{12}$ cm^{-2} and $n_2 = 9 \times 10^{12}$ cm^{-2}). Note that the $q^{\star}_{\rm op,ac}$ decreases with increasing ζ becoming zero in the limit $\zeta \to 1$. Since in this panel $\zeta \neq 0$ we have plotted both top-layer (low-density) and bottom-layer (high-density) Lindhard functions.

IV. DISCUSSION AND CONCLUSIONS

We have presented an analysis of the electronic collective modes of systems composed of two unhybridized but Coulomb-coupled MD2DESs separated by a vertical distance d. The primary example we have in mind is TI thin films, which are always described at low energies by this type of model because topologically protected MD2DESs always appear on both the top and bottom surfaces. Also of interest are closely related systems, which we refer to as DLG systems, containing two graphene layers that are weakly hybridized either because they are rotated relative to each other or because they are separated by a dielectric barrier layer. Importantly, we allow for a general dielectric environment in which the material

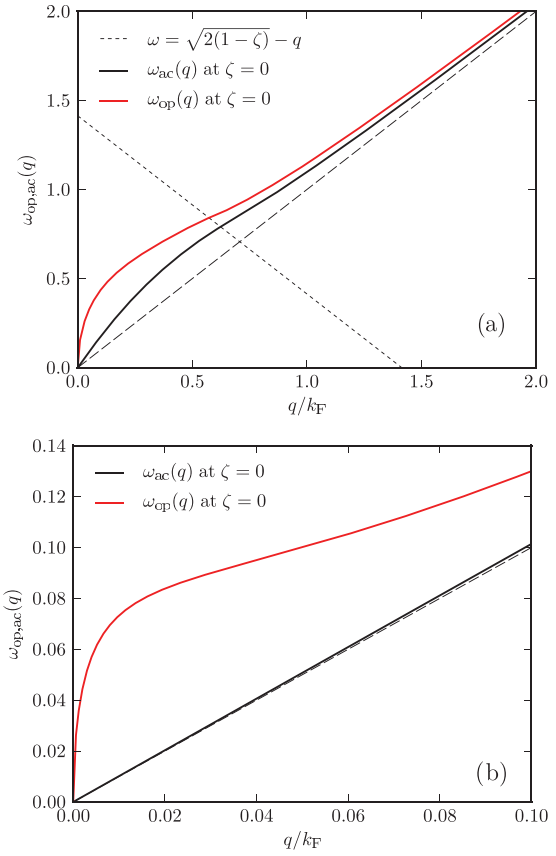

FIG. 5. (Color online) Optical and acoustic plasmon dispersions (in units of the Fermi energy $\varepsilon_F = vk_F$) in a double-layer graphene system [panel (a)] and a topological insulator thin-film [panel (b)] as functions of wave vector q [in units of $k_F = \sqrt{4\pi(n_1+n_2)/(g_s g_v)}$]. The intersections between the plasmon dispersions and the short-dashed line give the critical wave vector q_c at which Landau damping starts. Panel (a) The values of the parameters that we have used to produce the data in this figure are $g_s = g_v = 2$, $n_1 = n_2 = 5 \times 10^{12}$ cm^{-2} (corresponding to $n = 10^{13}$ cm^{-2} and $\zeta = 0$), $\alpha_{ee} = 2.2$, $d = 6$ nm, $\epsilon_1 = 1$, and $\epsilon_2 = \epsilon_3 = 4.0$. Panel (b) The values of the parameters that we have used to produce the data in this figure are $g_s = g_v = 1$, $n_1 = n_2 = 5 \times 10^{12}$ cm^{-2}, $\alpha_{ee} = 4.4$, $d = 6$ nm, $\epsilon_1 = 1$, $\epsilon_2 = 100$, and $\epsilon_3 = 4.0$. Note that due to the large value of the bulk TI dielectric constant, the acoustic plasmon is almost locked to the top of the intraband electron-hole continuum.

above the top MD2DES layer (ϵ_1), between the two layers (ϵ_2), and below the bottom MD2DES layer (ϵ_3) are all allowed to have different dielectric constants. In the case of TI thin film ϵ_2 is the bulk dielectric constant of the TI which is expected to have large values. The carrier collective modes of MD2DESs are expected to be most robust in the gap between intraband and interband particle-hole excitations.

The double-layer systems of interest quite generally have two collective modes which in the limit of small qd involve density fluctuations in the two layers that are strongly coupled and in the limit of large qd weakly coupled single-layer plasmons. One key parameter that controls collective mode properties is the dimensionless product $k_F d \equiv \bar{d}$. Small values of $k_F d$ imply that the layer separation is smaller than the typical distance between electrons within a layer and that collective modes at all values of q up to $\sim k_F$ are strongly coupled combinations of the two individual layer density-fluctuation contributions. For large $k_F d$ a crossover occurs for $q \in (0, k_F)$ between strongly and weakly coupled double-layer collective modes. Both small and large values of $\bar{d}$ are achievable in samples where disorder plays an inessential role in both DLG and TI thin-film cases.

Our study focuses on the long-wavelength limit in which both qd and $q/k_F = qd/\bar{d}$ are small. We have derived analytic expressions for both frequencies of both the low-energy linearly dispersing acoustic plasmon mode $\omega_{ac}(q)$ and for the high-energy optical plasmon mode $\omega_{op}(q)$ that has $\sqrt{q}$ dispersion at long wavelengths. In this limit we find that $\omega_{ac}(q) - vq \propto 1/\epsilon_2$, whereas $\omega_{op}(q) \propto \sqrt{2/(\epsilon_1+\epsilon_3)}$; i.e., the separation of the acoustic plasmon mode from the upper edge of the intraband particle-hole continuum is very strongly suppressed by a large bulk TI dielectric constant, whereas the coupled double-layer plasmon mode is unaffected. This double-layer optical plasmon behavior contrasts with that of a large qd single-surface plasmon mode that has a frequency proportional to $\sqrt{2/(\epsilon_2+\epsilon_{1,3})}$. The long-wavelength limit of $\omega_{ac}(q)$ is sensitive not only to the energy associated with interlayer charge sloshing but also to its microscopic kinetics as captured by the singular sensitivity of the MD2DES Lindhard function to $\omega/(vq)$. By carefully accounting for this dependence we are able to correct a previous analytic expression in a way that is quantitatively particularly important in the TI thin-film (large ϵ_2) case.

Double-layer collective mode coupling plays an important role in MD2DES correlations when $\bar{d}$ is small. Even when $\bar{d}$ is large, strongly coupled small $qd = q\bar{d}/k_F$ modes will often be experimentally accessible and may play an important role in graphene multilayer or TI-based plasmonics. The analytic results derived in this paper can be used to readily anticipate how these modes depend on system parameters.

From the more theoretical point of view, it will be intriguing to study physical properties of plasmons in Coulomb-coupled MD2DESs beyond the random-phase approximation by employing, e.g., many-body diagrammatic perturbation theory.[38]

While this manuscript was being finalized for publication, we have become aware of a study of optical and acoustic plasmons in double-layer graphene.[39] Moreover, the authors of this work state that the analytical result for the acoustic-plasmon group velocity given in Ref. 20 is incorrect (but give no analytical result for c_s) and present extensive numerical results for the "uniform medium" limit ($\epsilon_1 = \epsilon_2 = \epsilon_3$). An appendix in their work reports formal expressions for the general case $\epsilon_1 \neq \epsilon_2 \neq \epsilon_3$. The authors of Ref. 39 also include in their treatment retardation effects, which are unimportant, though, for the longitudinal plasmon modes studied in our paper.

ACKNOWLEDGMENTS

Work in Pisa was supported by the Italian Ministry of Education, University, and Research (MIUR) through the program "FIRB—Futuro in Ricerca 2010" Grant No. RBFR10M5BT (project title "PLASMOGRAPH: plasmons and terahertz devices in graphene"). A.H.M. was supported by Welch Foundation Grant No. TBF1473, DOE Division of Materials

Sciences and Engineering Grant No. DEFG03-02ER45958, and by the NRI SWAN program. M.P. acknowledges the kind hospitality of the IPM (Tehran, Iran) during the final stages of preparation of this work.

*asgari@ipm.ir
†m.polini@sns.it; http://qti.sns.it

[1]M. B. Pogrebinskii, Sov. Phys. Semicond. **11**, 372 (1977).
[2]P. J. Price, Physica B **117**, 750 (1983).
[3]A. K. Geim, Science **324**, 1530 (2009); A. H. Castro Neto, F. Guinea, N. M. R. Peres, K. S. Novoselov, and A. K. Geim, Rev. Mod. Phys. **81**, 109 (2009); A. K. Geim and K. S. Novoselov, Nat. Mater. **6**, 183 (2007).
[4]J. Moore, Nat. Phys. **5**, 378 (2009); J. E. Moore, Nature **464**, 194 (2010); M. Z. Hasan and C. L. Kane, Rev. Mod. Phys. **82**, 3045 (2010); X.-L. Qi and S.-C. Zhang, *ibid.* **83**, 1057 (2011).
[5]E. Rollings, G.-H. Gweon, S. Y. Zhou, B. S. Mun, J. L. McChesney, B. S. Hussain, A. V. Fedorov, P. N. First, W. A. de Heer, and A. Lanzara, J. Phys. Chem. Solids **67**, 2172 (2006); W. A. de Heer, C. Berger, X. Wu, P. N. First, E. H. Conrad, X. Li, T. Li, M. Sprinkle, J. Hass, M. L. Sadowski, M. Potemski, and G. Martinez, Solid State Commun. **143**, 92 (2007); P. N. First, W. A. de Heer, T. Seyller, C. Berger, J. A. Stroscio, and J.-S. Moon, MRS Bull. **35**, 296 (2010).
[6]See, for example, H. Zhang, C.-X. Liu, X.-L. Qi, Xi Dai, Z. Fang, and S.-C. Zhang, Nat. Phys. **5**, 438 (2009).
[7]S. Kim, I. Jo, J. Nah, Z. Yao, S. K. Banerjee, and E. Tutuc, Phys. Rev. B **83**, 161401 (2011).
[8]C. R. Dean, A. F. Young, I. Meric, C. Lee, L. Wang, S. Sorgenfrei, K. Watanabe, T. Taniguchi, P. Kim, K. L. Shepard, and J. Hone, Nat. Nanotechnol. **5**, 722 (2010).
[9]L. A. Ponomarenko, A. K. Geim, A. A. Zhukov, R. Jalil, S. V. Morozov, K. S. Novoselov, I. V. Grigorieva, E. H. Hill, V. V. Cheianov, V. I. Fal'ko, K. Watanabe, T. Taniguchi, and R. V. Gorbachev, Nat. Phys. **7**, 958 (2011).
[10]G. Li, A. Luican, and E. Y. Andrei, Phys. Rev. Lett. **102**, 176804 (2009); P. Neugebauer, M. Orlita, C. Faugeras, A.-L. Barra, and M. Potemski, *ibid.* **103**, 136403 (2009).
[11]G. Li, A. Luican, J. M. B. Lopes dos Santos, A. H. Castro Neto, A. Reina, J. Kong, and E. Y. Andrei, Nat. Phys. **6**, 109 (2009).
[12]H. Schmidt, T. Lüdtke, P. Barthold, E. McCann, V. I. Fal'ko, and R. J. Haug, Appl. Phys. Lett. **93**, 172108 (2008); H. Schmidt, T. Lüdtke, P. Barthold, and R. J. Haug, Phys. Rev. B **81**, 121403(R) (2010).
[13]The collective modes of bilayer graphene have already been calculated; see, e.g., G. Borghi, M. Polini, R. Asgari, and A. H. MacDonald, Phys. Rev. B **80**, 241402(R) (2009).
[14]See, for example, A. Bostwick, T. Ohta, T. Seyller, K. Horn, and E. Rotenberg, Nat. Phys. **3**, 36 (2007); Z. Q. Li, E. A. Henriksen, Z. Jiang, Z. Hao, M. C. Martin, P. Kim, H. L. Stormer, and D. N. Basov, *ibid.* **4**, 532 (2008); X. Du, I. Skachko, F. Duerr, A. Luican, and E. Y. Andrei, Nature **462**, 192 (2009); K. I. Bolotin, F. Ghahari, M. D. Shulman, H. L. Stormer, and P. Kim, *ibid.* **462**, 196 (2009); V. W. Brar, S. Wickenburg, M. Panlasigui, C.-H. Park, T. O. Wehling, Y. Zhang, R. Decker, C. Girit, A. V. Balatsky, S. G. Louie, A. Zettl, and M. F. Crommie, Phys. Rev. Lett. **104**, 036805 (2010); E. A. Henriksen, P. Cadden-Zimansky, Z. Jiang, Z. Q. Li, L.-C. Tung, M. E. Schwartz, M. Takita, Y.-J. Wang, P. Kim, and H. L. Stormer, *ibid.* **104**, 067404 (2010); A. Bostwick, F. Speck, T. Seyller, K. Horn, M. Polini, R. Asgari, A. H. MacDonald, and E. Rotenberg, Science **328**, 999 (2010); J. P. Reed, B. Uchoa, Y. I. Joe, Y. Gan, D. Casa, E. Fradkin, and P. Abbamonte, *ibid.* **330**, 805 (2010); A. Luican, G. Li, and E. Y. Andrei, Phys. Rev. B **83**, 041405(R) (2011); K. F. Mak, J. Shan, and T. F. Heinz, Phys. Rev. Lett. **106**, 046401 (2011); F. Ghahari, Y. Zhao, P. Cadden-Zimansky, K. Bolotin, and P. Kim, *ibid.* **106**, 046801 (2011); D. C. Elias, R. V. Gorbachev, A. S. Mayorov, S. V. Morozov, A. A. Zhukov, P. Blake, L. A. Ponomarenko, I. V. Grigorieva, K. S. Novoselov, F. Guinea, and A. K. Geim, Nat. Phys. **7**, 701 (2011); D. A. Siegel, C.-H. Park, C. Hwang, J. Deslippe, A. V. Fedorov, S. G. Louie, and A. Lanzara, Proc. Natl. Acad. Sci. USA **108**, 11365 (2011).
[15]D. Pines and P. Noziéres, *The Theory of Quantum Liquids* (W. A. Benjamin, Inc., New York, 1966).
[16]G. F. Giuliani and G. Vignale, *Quantum Theory of the Electron Liquid* (Cambridge University Press, Cambridge, 2005).
[17]S. A. Maier, *Plasmonics—Fundamentals and Applications* (Springer, New York, 2007).
[18]T. W. Ebbesen, C. Genet, and S. I. Bozhevolnyi, Phys. Today **61**, 44 (2008).
[19]F. H. L. Koppens, D. E. Chang, and F. J. García de Abajo, Nano Lett. **11**, 3370 (2011).
[20]E. H. Hwang and S. Das Sarma, Phys. Rev. B **80**, 205405 (2009).
[21]S. Raghu, S. B. Chung, X. L. Qi, and S.-C. Zhang, Phys. Rev. Lett. **104**, 116401 (2010).
[22]Yu. E. Lozovik and A. A. Sokolik, JETP Lett. **87**, 61 (2008); Yu. E. Lozovik, S. L. Ogarkov, and A. A. Sokolik, Phil. Trans. Roy. Soc. A **368**, 5417 (2010).
[23]For a recent review, see, e.g., V. Pellegrini and A. Pinczuk, Phys. Status Solidi B **243**, 3617 (2006).
[24]D. S. Kainth, D. Richards, H. P. Hughes, M. Y. Simmons, and D. A. Ritchie, Phys. Rev. B **57**, 2065(R) (1998); D. S. Kainth, D. Richards, A. S. Bhatti, H. P. Hughes, M. Y. Simmons, E. H. Linfield, and D. A. Ritchie, *ibid.* **59**, 2095 (1999); D. S. Kainth, D. Richards, H. P. Hughes, M. Y. Simmons, and D. A. Ritchie, J. Phys. Condens. Matter **12**, 439 (2000); C. F. Hirjibehedin, A. Pinczuk, B. S. Dennis, L. N. Pfeiffer, and K. W. West, Phys. Rev. B **65**, 161309 (2002); S. V. Tovstonog, L. V. Kulik, I. V. Kukushkin, A. V. Chaplik, J. H. Smet, K. V. Klitzing, D. Schuh, and G. Abstreiter, *ibid.* **66**, 241308 (2002).
[25]Y. Liu, R. F. Willis, K. V. Emtsev, and T. Seyller, Phys. Rev. B **78**, 201403(R) (2008); Y. Liu and R. F. Willis, *ibid.* **81**, 081406(R) (2010); R. J. Koch, T. Seyller, and J. A. Schaefer, *ibid.* **82**, 201413(R) (2010); T. Langer, J. Baringhaus, H. Pfnür, H. W. Schumacher, and C. Tegenkamp, New J. Phys. **12**, 033017 (2010); C. Tegenkamp, H. Pfnür, T. Langer, J. Baringhaus, and H. W. Schumacher, J. Phys. Condens. Matter **23**, 012001 (2011); S. Y. Shin, C. G. Hwang, S. J. Sung, N. D. Kim, H. S. Kim, and J. W. Chung, Phys. Rev. B **83**, 161403(R) (2011).

[26]X. G. Peralta, S. J. Allen, M. C. Wanke, N. E. Harff, J. A. Simmons, M. P. Lilly, J. L. Reno, P. J. Burke, and J. P. Eisenstein, Appl. Phys. Lett. **81**, 1627 (2002).
[27]L. Ju, B. Geng, J. Horng, C. Girit, M. Martin, Z. Hao, H. A. Bechtel, X. Liang, A. Zettl, Y. R. Shen, and F. Wang, Nat. Nanotechnol. **6**, 630 (2011).
[28]Z. Fei, G. O. Andreev, W. Bao, L. M. Zhang, A. S. McLeod, C. Wang, M. K. Stewart, Z. Zhao, G. Dominguez, M. Thiemens, M. M. Fogler, M. J. Tauber, A. H. Castro-Neto, C. N. Lau, F. Keilmann, and D. N. Basov, Nano Lett. **11**, 4701 (2011).
[29]R. E. V. Profumo, M. Polini, R. Asgari, R. Fazio, and A. H. MacDonald, Phys. Rev. B **82**, 085443 (2010).
[30]B. Wunsch, T. Stauber, F. Sols, and F. Guinea, New J. Phys. **8**, 318 (2006).
[31]E. H. Hwang and S. Das Sarma, Phys. Rev. B **75**, 205418 (2007).
[32]Y. Barlas, T. Pereg-Barnea, M. Polini, R. Asgari, and A. H. MacDonald, Phys. Rev. Lett. **98**, 236601 (2007).
[33]S. Das Sarma and A. Madhukar, Phys. Rev. B **23**, 805 (1981).
[34]G. E. Santoro and G. F. Giuliani, Phys. Rev. B **37**, 937 (1988).
[35]M. Polini, R. Asgari, G. Borghi, Y. Barlas, T. Pereg-Barnea, and A. H. MacDonald, Phys. Rev. B **77**, 081411(R) (2008).
[36]W. Richter and C. R. Becker, Phys. Status Solidi B **84**, 619 (1977).
[37]D. L. Miller *et al*., Science **324**, 924 (2009); J. M. B. Lopes dos Santos, N. M. R. Peres, and A. H. Castro Neto, Phys. Rev. Lett. **99**, 256802 (2007).
[38]S. H. Abedinpour, G. Vignale, A. Principi, M. Polini, W.-K. Tse, and A. H. MacDonald, Phys. Rev. B **84**, 045429 (2011).
[39]T. Stauber and G. Gómez-Santos, Phys. Rev. B **85**, 075410 (2012).